Supplementary Information

Leveraging the Cooperative Photocatalysis for the Concurrent Production of Solar Fuel and Value-added Chemicals: Mediated by the Metal-free Porphyrin-based Polymeric Framework

Kirti Dhingra, Neha Saini, Amit Kumar, Kamalakannan Kailasam*

Advanced Functional Nanomaterials, Institute of Nano Science and Technology (INST), Knowledge City, Sector-81, Manauli, SAS Nagar, 140306 Mohali, Punjab, India.

***Email:**kamal@inst.ac.in*

1. Experimental Section

1.1 Chemicals and Materials

4,4'-(thiazolo[5,4-d]thiazole-2,5-diyl)dibenzaldehyde (Tz) was synthesized as per the reported literature[1]. 5,10,15,20-tetrakis (4-aminophenyl) porphyrin (Porp), acetic acid (AcOH), n-butanol (n-BuOH), benzylamine, and its substrates, 1,2,3,4- tetrahydroisoquinoline, and its substrates were purchased from the Tokyo Chemical Industry Co., Ltd. (TCI). Acetonitrile (ACN), o-dichlorobenzene (o-DCB), tetrahydrofuran (THF), dithioxamide, dimethylformamide, and deuterated organic solvents were procured from Sigma-Aldrich. Commercially available chemicals, solvents, and reagents were employed without further purification.

1.2 Synthesis of Tz-CHO

4,4'-(thiazolo[5,4-d] thiazole-2,5-diyl)dibenzaldehyde (Tz-CHO) was synthesized by adding a solution of dithiooxamide (30.0 mg, 0.5 mmol) in 7 ml DMF to the solution of 1,4-phthalaldehyde (340.0 mg, 5.0 mmol) in 20 ml of DMF dropwise and after addition the mixture was heated to 150 ºC for 5 h.[1] The bright orange-coloured precipitates of Tz-CHO were collected and purified through column chromatography. Yield 49%, ^{1}H NMR (500 MHz, $CDCl_3$): 8.31 (d, 4H), 7.89 (d, 4H), 10.01 (s, 2H). ^{13}C CP/MAS NMR:δ 190, 168, 153, 151, 137, 134, 128, 126.

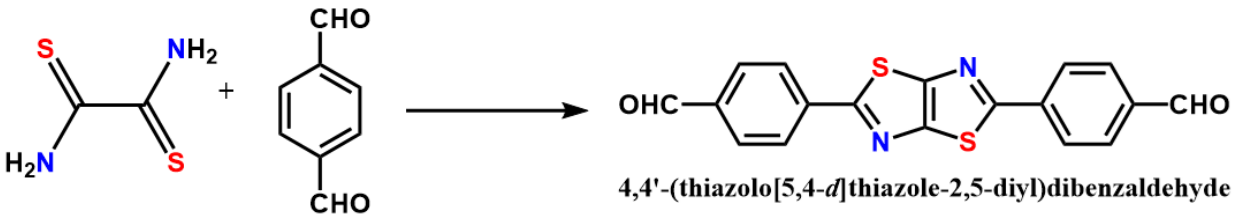

Synthesis scheme

1.3. Synthesis of Porp-Tz

For the synthesis of Porp-Tz POP, a 25 ml glass ampoule was charged with a tetratopic amine, 5,10,15,20-tetrakis (4-aminophenyl) porphyrin (Porp-NH_2) (0.08 mmol) and a ditopic aldehyde, 4,4'-(thiazolo[5,4-d] thiazole-2,5-diyl) dibenzaldehyde (Tz-CHO) (0.04 mmol). A mixed solvent of o-dichlorobenzene (o-DCB):n-butanol (n-BuOH) (1:1 ratio) was added (Synthesis **Scheme 1**), and the reaction mixture was sonicated for 10 min to obtain a homogenous mixture followed by the slow addition of 0.4 mL of 8 M acetic acid (AcOH). Further, the homogenous mixture was degassed through three cycles of freeze-pump-thaw, and the ampoule was flame-sealed under vacuum. After that, the ampoule was heated in an oven at 120 ºC for four days and cooled to room temperature. The reaction mixture was filtered and the resulting dark brown precipitates were collected in a Whatman filter paper and subjected to consequent washings with several organic and aqueous solvents such as isopropanol, acetone, methanol, tetrahydrofuran, dimethylsulfoxide, 1,4-dioxane, dichloromethane, and water to remove the residual starting materials. Further, purification was carried out by the soxhlet extraction in methanol: THF (1:1) for 3 days followed by drying at 100 °C for 12 h in a vacuum oven. Other reaction conditions were optimized to obtain the highest surface area as shown in **Table S2**.

2. Characterization

After synthesizing the POP, the basic structural characterization was carried out by recording Fourier-transform infrared (FT-IR) spectroscopy analysis on Bruker Vertex FT-IR 70/80 spectrometer in the 4000-400 cm^{-1} spectral range. To further confirm the structure, ^{13}C

cross-polarization magic angle spinning (CP/MAS) solid-state NMR experiment was performed on the Bruker Avance NEO 400 using a 5 mm FG NMR probe. Elemental analysis was carried out using an Elementar Vario MACRO cube elemental analyzer. After the complete structural analysis, the N_2 physisorption measurements were performed on an Autosorb iQ3 instrument (Quantachrome) at 77 K after the sample was degassed for 12 h at 120 ºC. The specific surface area of the polymeric network was analyzed using the Brunauer-Emmett-Teller (BET) micropore-assisted method and for the estimation of pore size distribution, the nonlinear density functional theory (NLDFT) method was used. The morphological aspect of the polymeric network was carried out using Field emission scanning electron microscope (FESEM) and Transmission electron microscope (TEM) analysis employing JEOL JSM-7610F Plus instrument and JEOL JEM-2100 operated at an accelerating voltage of 120 kV, respectively. To identify the elemental composition of the sample as well as their chemical states or the complete electronic structure, X-ray photoelectron spectroscopy (XPS) was employed by using an Al Kα X-ray source and a monochromator with ultra-high vacuum (7 x 10^{-9} torr) manufactured by Thermo Fisher Scientific. Powder X-ray diffraction (PXRD) analytical techniques was used for the measurement of the diffraction pattern. For PXRD, a PAN analytical's X'PERT PRO X-ray diffractometer having Cu-Kα radiation (λ = 0.15418 Å, 2θ = 2-40°) source operating at 40 kV and 20 mA was employed. The optical properties of the sample (absorbance spectra) were recorded on an Agilent Cary 100 UV-Vis spectrophotometer. Horiba Fluorolog instrument was used to record the sample's solid-state Photoluminescence spectra (PL) and examine the time-resolved photoluminescence emissions. All the electrochemical studies were carried out at the standard three-electrode electrochemical workstation, Metrohm Autolab (M204 multichannel potentiostat galvanostat). The Pt electrode was used as a counter electrode, Ag/AgCl (in saturated KCl) as a reference electrode, and a glassy carbon electrode with the sample drop cast as a thin paste (ethanol and Nafion) was employed as a working electrode. 0.2 M Na_2SO_4 was used as an electrolyte to carry out all the electrochemical measurements.

Thermogravimetric analysis (TGA) was done under an inert atmosphere using a SHIMADZU DTG-60H analyzer (flow rate of 20 mL/min) with a temperature ranging from 30 to 1000 °C. The Electron Paramagnetic Resonance (EPR) experiment was performed at room temperature by Bruker A300-9.5/12/S/W. After the catalytic reaction, the qualitative and

quantitative analysis of the liquid product was done by Shimadzu Gas Chromatography-Mass Spectrometer (GC-MS). The yield of H_2O_2 was calculated by the iodometry method using UV-vis spectroscopy.

3. Photocatalytic Experiments

The photocatalytic H_2O_2 production coupled with aerobic oxidation reactions was performed in a glass round bottom flask under a 23 W White LED. Typically, 5 mg of the catalyst and the substrate were dispersed in acetonitrile (ACN) solvent and the round bottom flask was sealed using a rubber septum. The reaction mixture was purged with O_2 for 10 min using a balloon (atmospheric pressure) in dark conditions until saturation and illuminated by a table lamp (23 W white LED). Upon the completion of the reaction, the catalyst was separated from the reaction mixture by a microcentrifuge, washed with ethanol, and dried at 100 ºC in a vacuum oven to be used further for successive photocatalytic cycles.

4. H_2O_2 measurements

The iodometry-based method was employed for the quantitative detection of the H_2O_2 generated. 450 µL of 0.4 mol L^{-1} (0.4 M) potassium iodide aqueous solution and 450 µL of 0.1 mol L^{-1} (0.1 M) potassium hydrogen phthalate aqueous solution was mixed in a 1.0 mL plastic vial followed by the addition of 100 µL of the filtered reaction mixture. The resultant aqueous mixture was kept for 30 min with the aluminium foil wrapped around it. The H_2O_2 oxidizes the iodide ions (I^-) under the acidic conditions to triiodide ions (I^{3-}). The mixture was diluted 100 times and the absorbance was measured by the UV-Vis spectrometer. The amount of H_2O_2 formed was quantified by calculating the absorbance of triiodide ions at 350 nm.

5. $HO^{\cdot}$ detection

For the detection of $HO^{\cdot}$, the PL emission technique has been employed by taking terephthalic acid (TA) as the probe molecule. Upon irradiation with the light, TA reacts with $HO^{\cdot}$ to give 2-hydroxy terephthalic acid in the presence of NaOH which was observed by an increase in the PL emission intensity at 425 nm with time.

6. Calculation of Apparent Quantum Yield (AQY%)

The apparent quantum yield (AQY) is the number of electrons reacted to the total number of photons incident on the catalyst surface, it gives an idea about the photocatalytic performance of the catalyst.[22]

$$AQY\ (\%) = \frac{Number\ of\ reacted\ electrons}{Number\ of\ incident\ photons} \times 100$$

For the H_2O_2 production, AQY was estimated by irradiating 5 mg Porp-Tz with 400 W Xe lamp using different band-pass filters for 1 h.

$$AQY\ (\%) = \frac{2 \times Number\ of\ of\ \ H_2O_2\ produced}{Number\ of\ incident\ photons} \times 100$$

The number of incident photons is the ratio of the total incident energy to the energy of the single photon, and the total energy of the incident light,

$$E_{total} = I \times A\ \times t$$

I = Intensity of the incident light (Wcm^{-2})

A = Area of irradiation (cm^2)

t = Time of irradiation (s)

The energy of one photon is given by, $E_{photon} = \frac{hc}{\lambda_{inc}}$

h = Planck's constant (Js)

c = Speed of light (ms^{-1})

λ_{inc} = Wavelength of the monochromatic light (m)

and, the number of H_2O_2 generated = $\eta_{H_2O_2}$× Avogadro number (N_A)

By putting both the energy values for the calculation of the total number of incident photons and the number of H_2O_2 generated, AQY (%) is as depicted by the equation,

$$AQY\ (\%) = \frac{2 \times \eta_{H_2O_2} \times N_A \times h \times c}{I \times A \times t \times \lambda_{inc}} \times 100$$

where, $\eta_{H_2O_2}$ is the number of moles of H_2O_2 generated upon irradiation of incident light for the 't' time duration.

6. Supplementary Figures

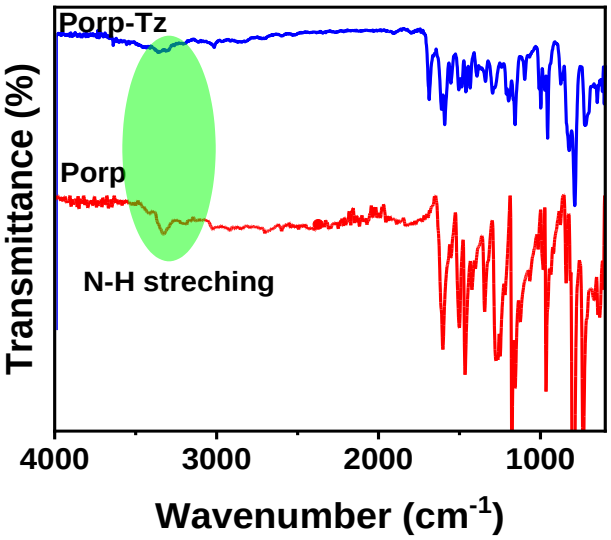

Fig. S1: The FTIR pattern comparing Porp and Porp-Tz.

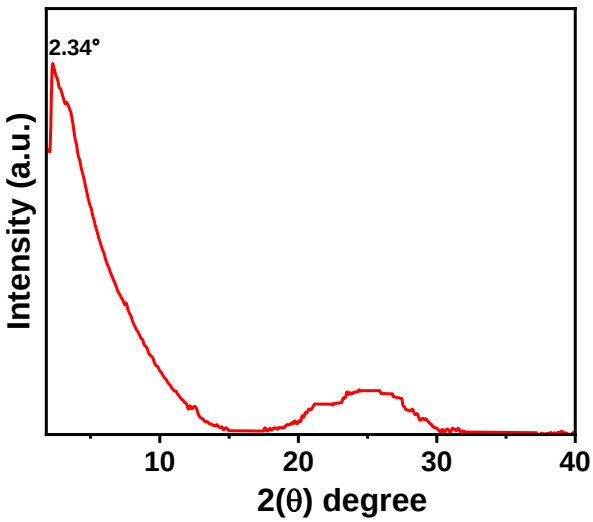

Fig. S2: The PXRD pattern of Porp-Tz.

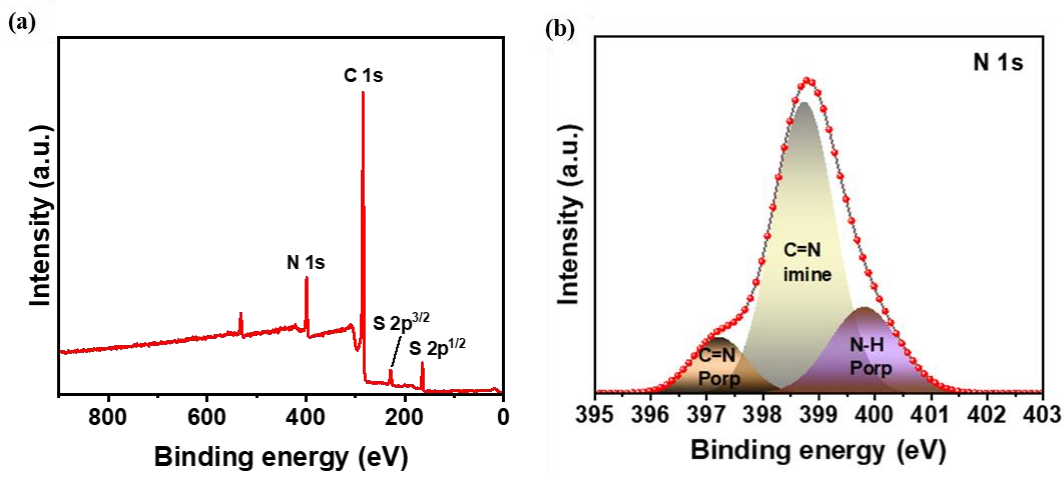

Fig. S3: (a) XPS survey scan; and (b) N 1s high-resolution XPS spectra of Porp-Tz.

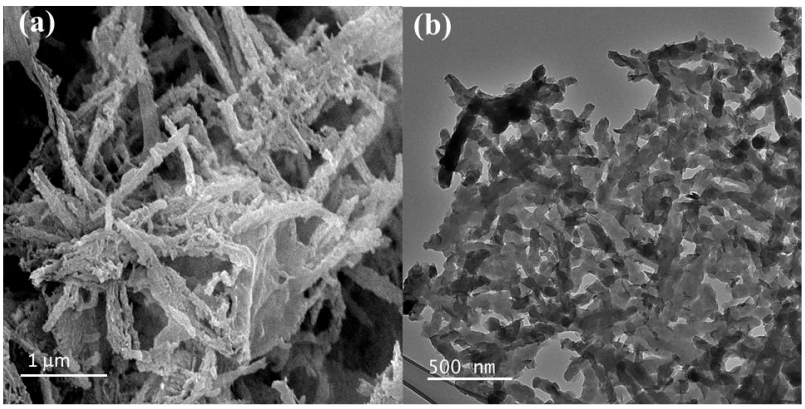

Fig. S4: (a) FESEM; and (b) TEM images of Porp-Tz polymeric network.

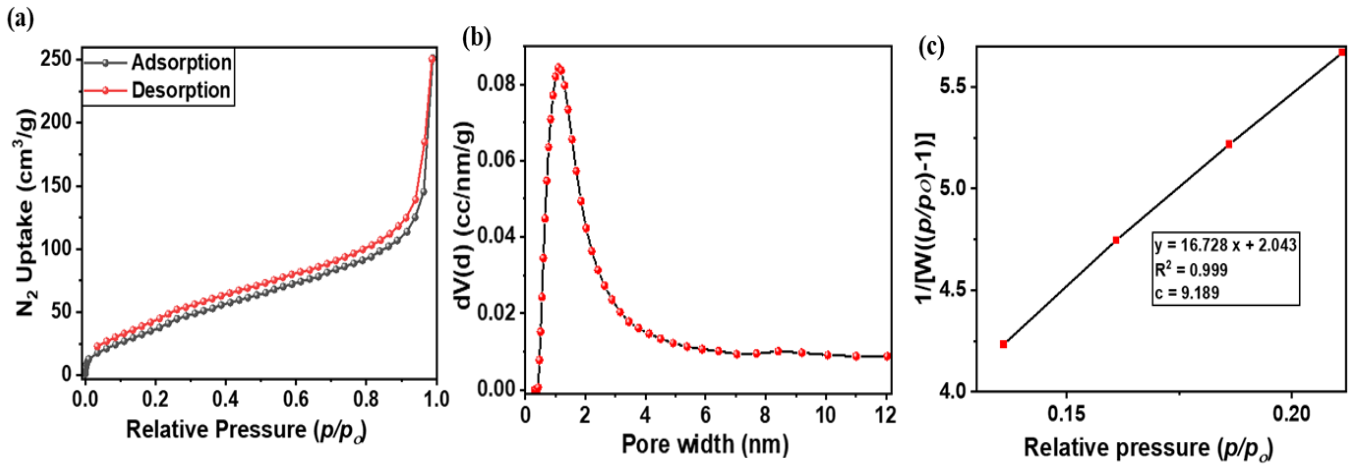

Fig. S5: (a) N_2 adsorption and desorption isotherm; (b) Pore size distribution; and (c) Linear BET plot of Porp-Tz.

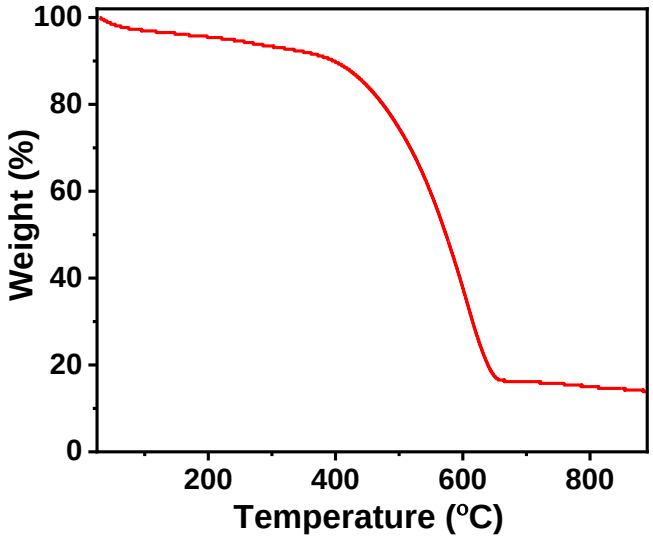

Fig. S6: TGA profile of Porp-Tz under nitrogen atmosphere.

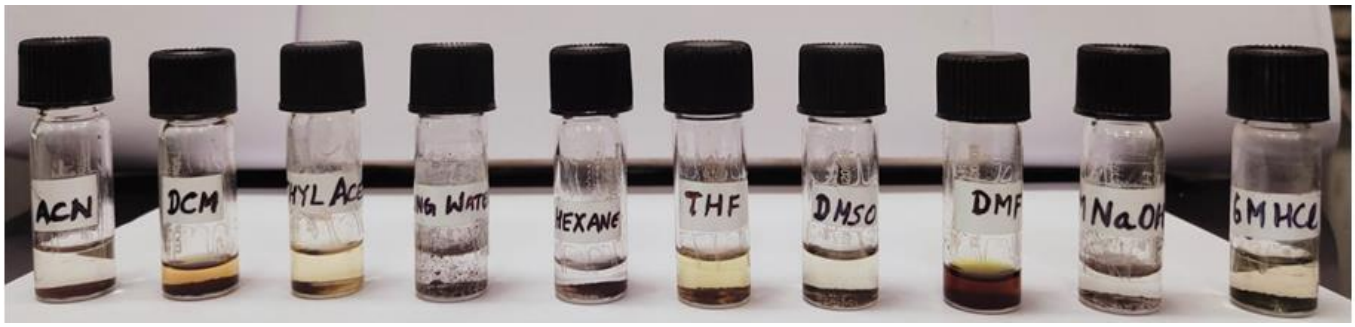

Fig. S7: Porp-Tz after immersion in different solvents; 6 M NaOH; and 6 M HCl for 3 days.

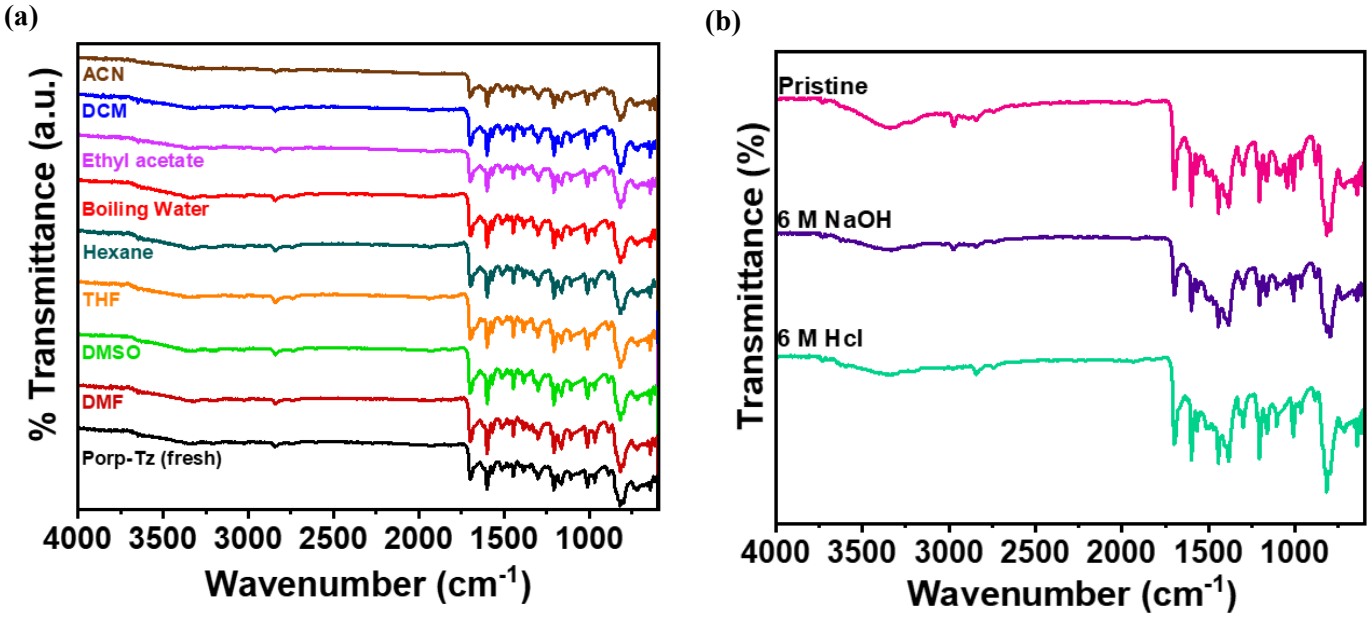

Fig. S8: FTIR spectra of Porp-Tz after immersion for 3 days in (a) different solvents; (b) 6 M HCl; and 6 M NaOH.

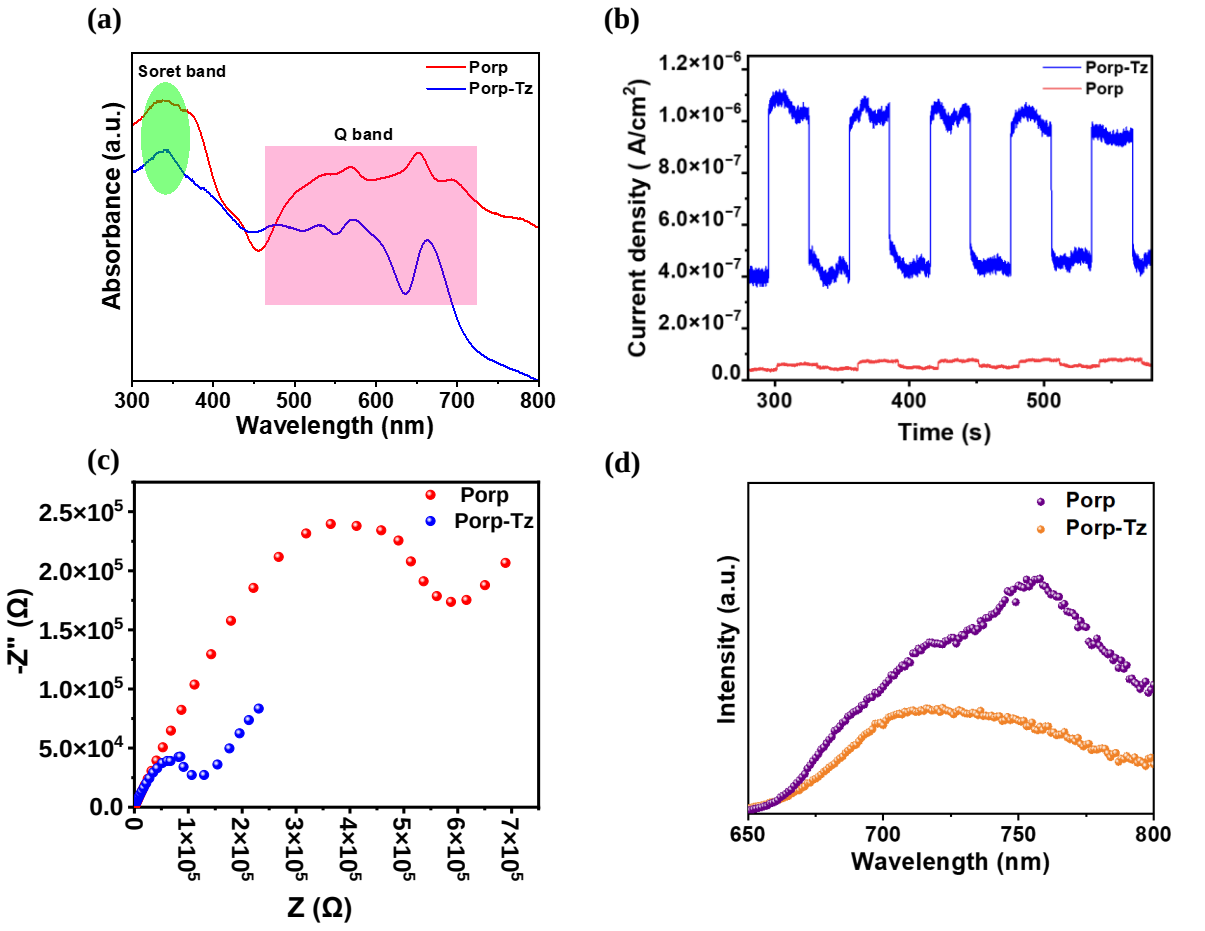

Fig. S9: Comparative studies of Porp and Porp-Tz (a) DR UV-vis spectra, (b) Transient PC studies, (c) Nyquist plot, and (d) PL spectra.

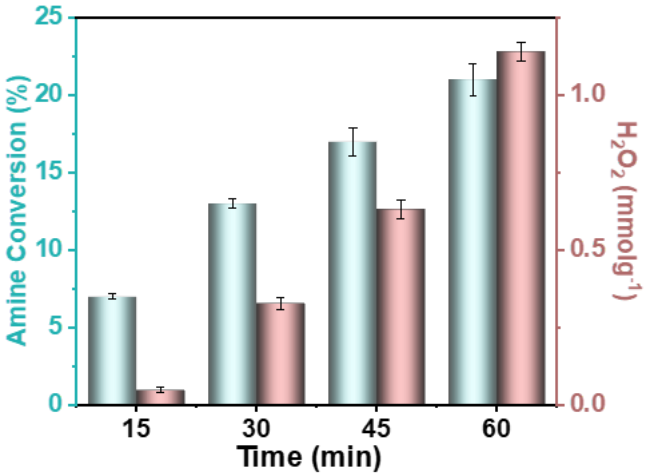

Fig. S10: Time-dependent study for the benzylamine homocoupling of Porp (monomer) as photocatalyst.

Heterocoupling of Benzylamine and Benzaldehyde

For the heterocoupling reaction, 5 mg of the catalyst, 1 mmol of benzyl alcohol, and 1 mmol of benzylamine were dispersed in acetonitrile (ACN) solvent. The reaction mixture was purged with O_2 for 10 min using a balloon (atmospheric pressure) in dark conditions until saturation and then irradiated by a 23 W white LED. Upon the completion of the reaction, the catalyst was separated from the reaction mixture by a microcentrifuge, washed with ethanol, and dried at 100 ºC in a vacuum oven.

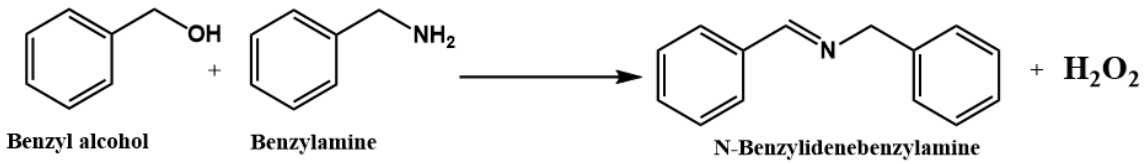

Reaction Conditions: Porp-Tz (5 mg); Benzyl amine (1 mmol); Benzyl alcohol (1 mmol); ACN (20 ml); O_2; RT; 1 h; and White LED (23 W).

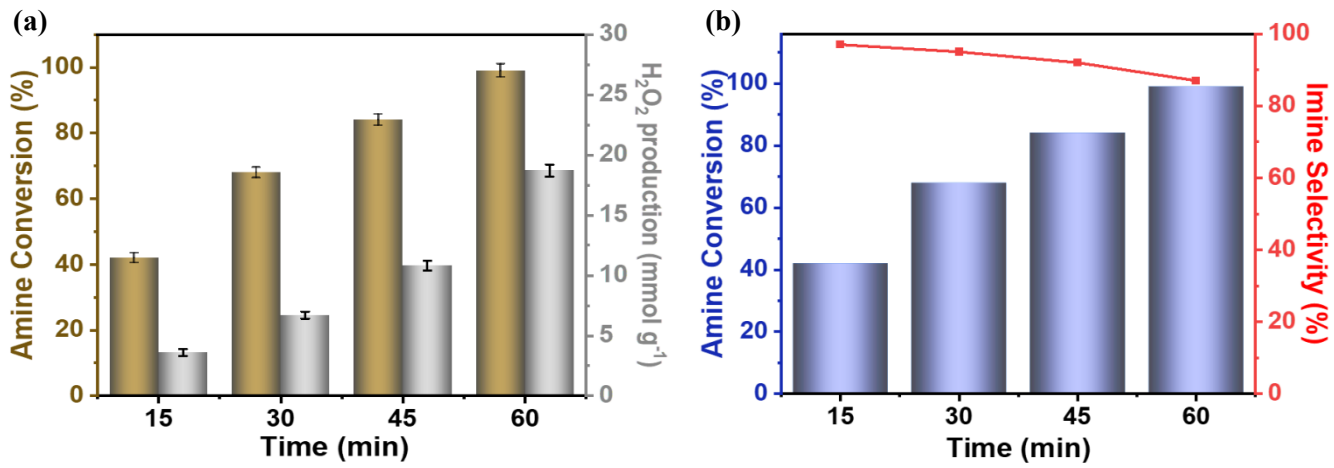

Fig. S11: Heterocoupling time study experiment graphs of Porp-Tz for (a) amine conversion and H_2O_2 (mmol g^{-1}); and (b) amine conversion and selectivity of N-bezylidenebenzylamine formed.

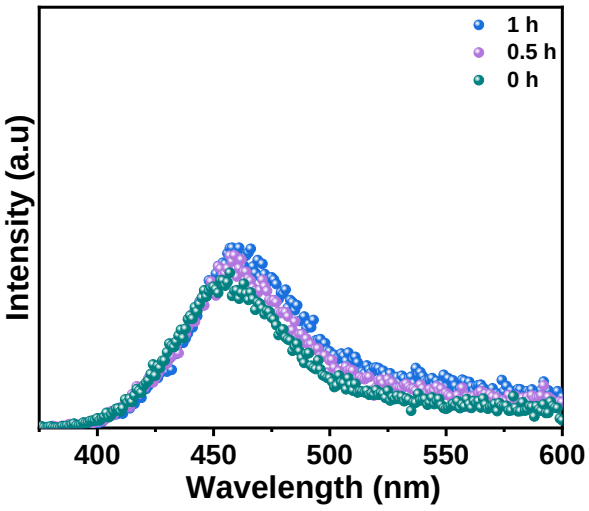

Fig. S12: Dynamic spectra of photo-hydroxylation of terephthalic acid with time.

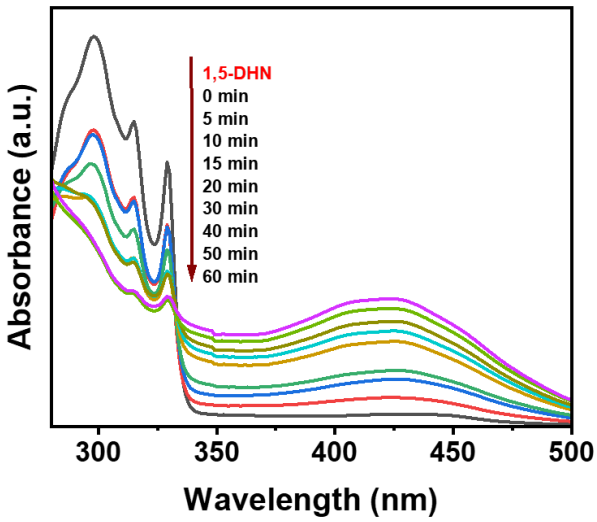

Fig. S13: Dynamic spectra of photo-oxidation of 1,5-DHN to Juglone with time.

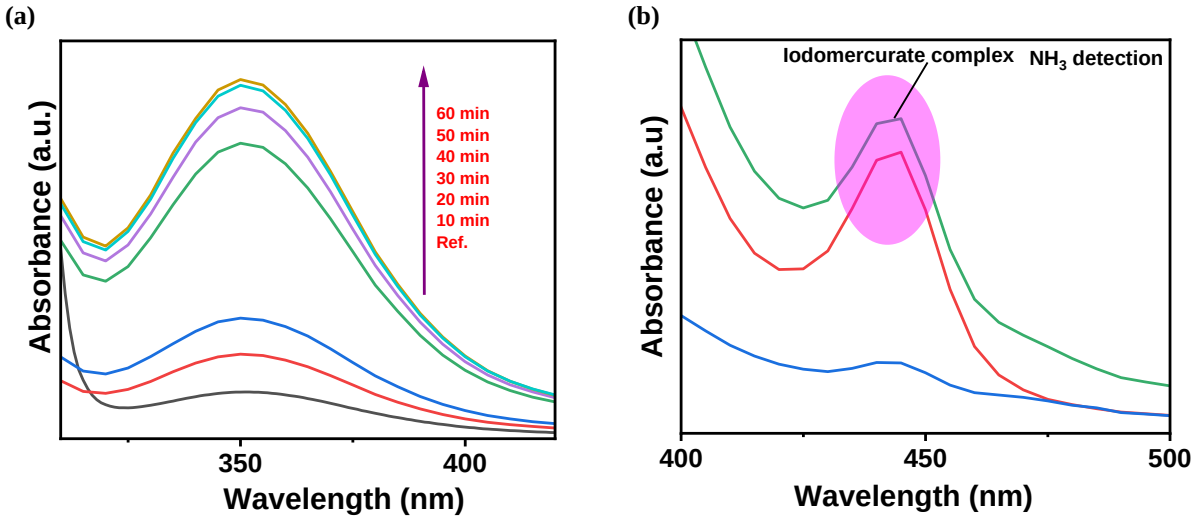

Fig. S14: UV-vis absorption spectra of Porp-Tz (a) with time depicting H_2O_2 production, and (b) NH_3 detection.

Fig. S15: GC-MS chromatogram for the benzylamine

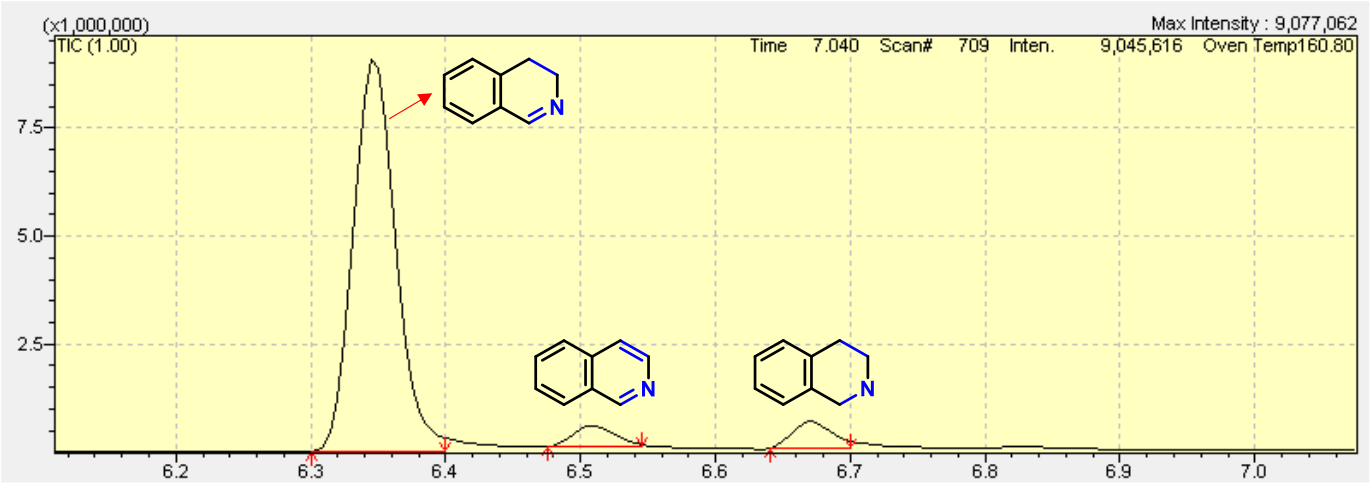

Fig. S16: GC-MS chromatogram of the for the dehydrogenation of THIQs.

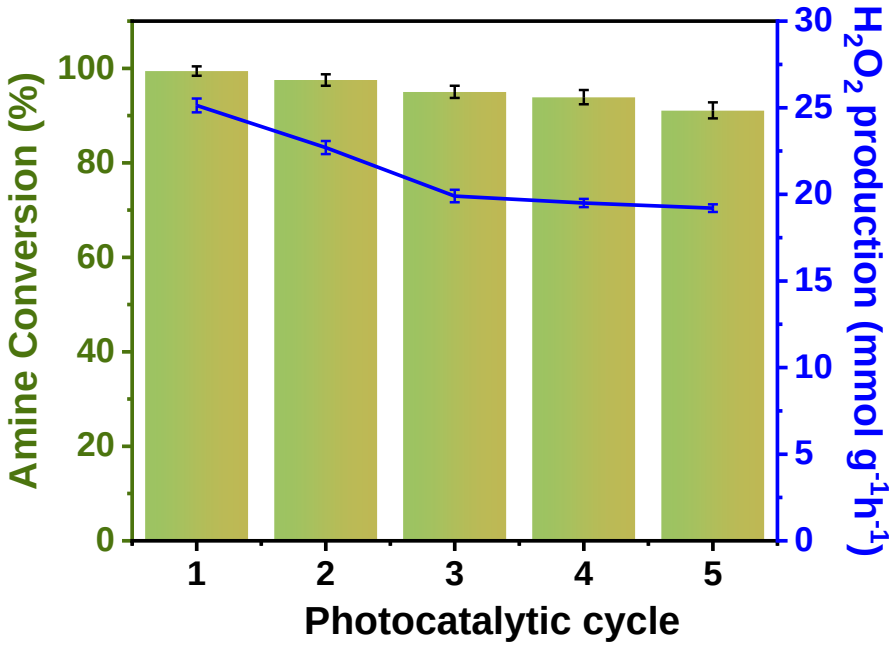

Fig. S17: The photocatalytic performance of Porp-Tz for five consecutive cycles.

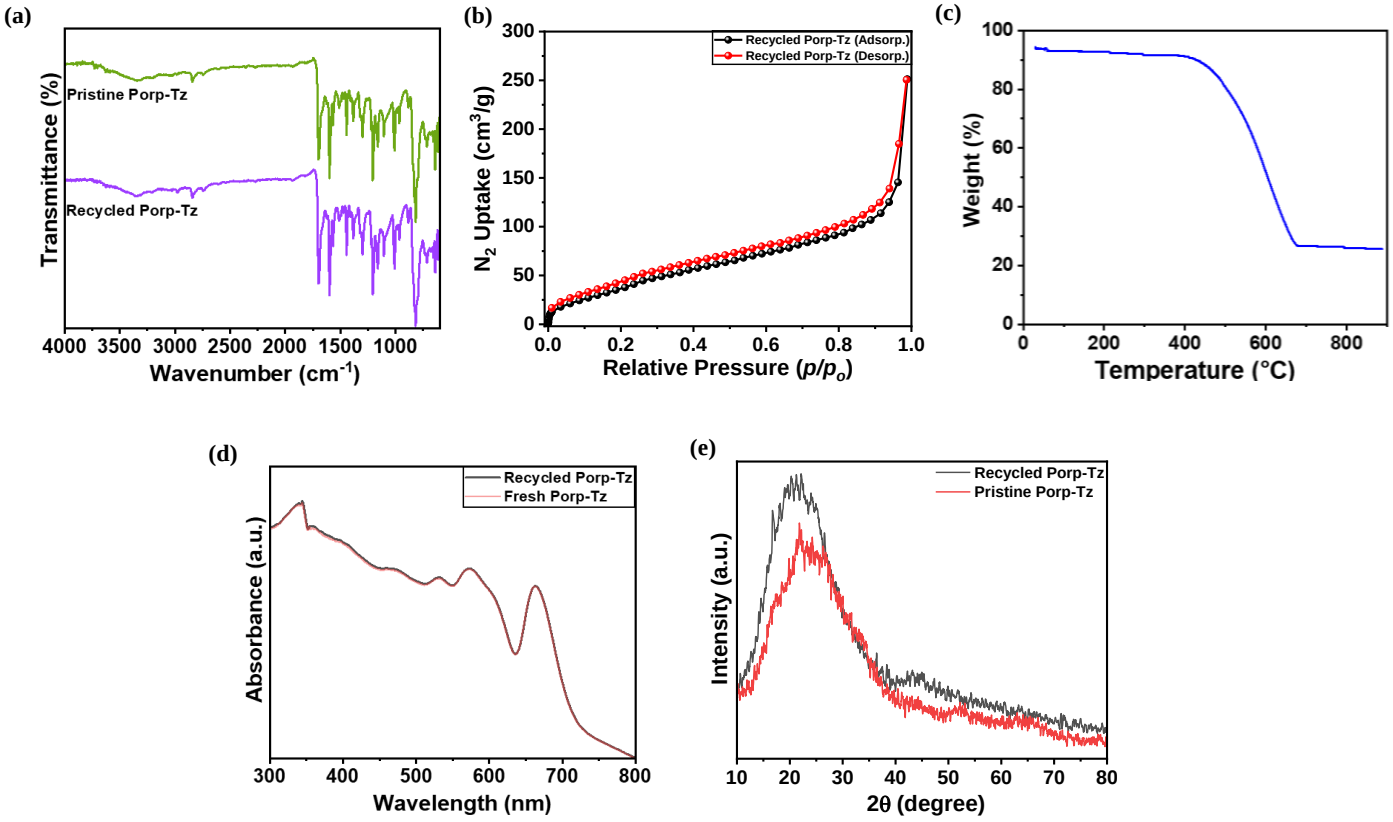

Fig. S18: After recyclability experiments of Porp-Tz: (a) FTIR spectra, (b) N_2 sorption isotherm, (c) TGA plot, (d) DR UV-vis spectra, and (e) PXRD pattern.

7. Supplementary Tables

Table S1: Comparison table showing previously reported photocatalysis for the concurrent production of H_2O_2 and the value-added fine chemical.

S.No	Catalyst/ Amount (mg)	Reaction Conditions	Light Source	Reaction Products		Ref.
				Oxi^n product/ Conv. (% Sel.)	**Red^n product (H_2O_2 prod rate in mmol g^{-1} h^{-1})**	
1	**Porp-Tz/ 5mg**	**1 mmol Benzylamine, 20 mL ACN, O_2, 1 h**	**23 W white LED**	**Benzonitrile/ 99.9 (>99)**	**25.13**	**This Work**
2	**Porp-Tz/ 5 mg**	**1 mmol THIQs, 20 mL ACN, O_2, 2 h**	**23 W white LED**	**DHIQs/ 91 (96)**	**13.34**	
Metal-free Photocatalysts						
3	CTF-Th/ 50 mg	30 mL of Toluene/ACN (1:1), O_2, 3 h	AM 1.5 G simulated sunlight	Benzaldehyde/ 2.25 mmol (>99)	0.7	3
4	g-C_3N_4/ 20 mg	Ethanol/H_2O (9:1), O_2, 12 h	300 W Xe-lamp, λ>420 nm	Aldehyde/ 0.032 mmol (90)	0.125	4
5	NCN/ 20 mg	Lactic acid, O_2, 5 h	300 W Xe-lamp	Pyruvic acid/9.7 % (>70)	32.8	5
6	DCM-HCPs/ 10 mg	0.2 mmol benzylamine, 10 mL ACN, Air, 1.5 h	455 nm Blue LED lamp	Benzonitrile, 99.8 % (>99.9)	5.71	6
7	H_3LP-HCPs/ 10 mg	0.2 mmol of benzylamine, 10 mL CH_3CN, air, 0.83 h	455 nm Blue LED	Benzonitrile/ >99 % (>99)	9.2	7
8	H_6P-HCPs/ 15 mg	BA/H_2O (2:3), O_2, 3h	300 W Xe-lamp λ>420 nm	Benzaldehyde/ 100 % (96)	29.26	8
Metal-based Photocatalysts						
9	TBCN@3 %rGO/ 20 mg	0.2 mmol benzyl alcohol, O_2, 1 h	250 W White LED	Benzaldehyde/ 92.1 % (98.2)	8.6	9
10	OPA/Fe-Zr-MOF / 5 mg	48.1 mmol benzyl alcohol, O_2, 3 h	500 W Xe lamp, λ>420 nm	Benzaldehyde/ 0.12 mmol (>99)	5.24	10
11	OPA/ $Zr_{92.5}Ti_{7.5}$-MOF/ 5 mg	Benzyl alcohol: H_2O (5 mL:2 mL), O_2, 3 h	500 W Xe lamp, λ>420 nm	Benzaldehyde/ 0.1 mmol (>99)	1.51	11
12	$CdIn_2S_4$/ 20 mg	1 mL benzylamine, 50 mL water, O_2, 4 h	300 W Xe-lamp, λ>420 nm	Benzonitrile/ 11.8 mmol (>99)	12.26	12

13	$ZrS_{1-y}S_{2-x}$ (15/100) NB_s/ 50 mg	0.1 mmol benzylamine, 30 mL water, O_2, 5 h	AM 1.5G simulated sunlight	Benzonitrile/ 0.16 mmol (>99)	1.56	13
14	$Zn_3In_2S_6$ / 5 mg	0.125 mmol THIQs, O_2, 20 min	Xe lamp, λ ≥ 400 nm	DHIQs/ 90 % (92.1)	66.4	2
15	Fe_3O_4@CdS@CQDs/ 5 mg	Benzyl alcohol, 10 mL ACN, O_2, 4 h	Xe lamp, λ>300 nm	Benzaldehyde/ 1.14 mmol (>99)	27.06	14
16	TiO_2/ 50 mg	1.75 mmol benzyl alcohol, O_2, 12 h	450 W Hg lamp, λ>280 nm	Aldehyde/ 0.397 mmol (>99)	20	15
17	TBO40/ 20 mg	0.29 mmol furfuryl alcohol, O_2, 12 h	300 W Xe lamp, λ>350 nm	Furoic acid/ 0.27 mmol (>99)	2.9	16
18	Co_9S_8-$CoZnIn_2S_4$ / 10 mg	H_2O /Benzyl alcohol (5:2), O_2, 5 h	300 W Xenon lamp λ>420 nm	Benzaldehyde/ 1594 mmol (>99)	34	17
19	Bi_2MoO_6-H_2-2/ 5 mg	0.05 mmol benzyl alcohol, 2 mL acetonitrile, Air, 5 h	300 W Xe lamp, λ>320 nm	Benzaldehyde / 72 % (91)	0.07	18

Table S2: Comparison table showing the photocatalytic H_2O_2 production based on organic polymer and sacrificial agents.

S.No	Catalyst/ Amount (mg)	Reaction Conditions	Sacrificial agent	H_2O_2 prod rate (mmol g^{-1} h^{-1})	References
1	**Porp-Tz/ 5mg**	**1 mmol Benzylamine ,20 mL ACN, O_2, 1 h, 23 W white LED**	**Benzylamine**	**25.13**	**This Work**
2	**Porp-Tz/ 5 mg**	**1 mmol THIQs, 20 mL ACN, O_2, 2 h, 23 W white LED**	**THIQs**	**13.34**	
3	HEP-TAPT-COF/ 50 mg	100 mL H_2O, 300 W Xe-lamp, λ>420 nm, O_2	-	1.75	19
4	N_0-COF/ 20 mg	100 mL H_2O, 495 nm LED, O_2	-	0.14	20
5	COF-TfpBpy/ 20 mg	100 mL H_2O, Xe-lamp λ>420 nm, air	-	10.42	21
6	SonoCOF-F_2/ 3 mg	H_2O/ benzyl alcohol (9:1), 1.5 h, Oriel Solar Simulator, O_2	-	2.42	22

7	RF523/ 50 mg	40 mL H_2O,523 K, 24 h, AM1.5G simulated sunlight, O_2	-	0.13	[23]
8	TACOF-1-COOH/ 2.5 mg	18 mL H_2O,10 vol% ethanol, 300 W Xe lamp, O_2	-	6.61	[24]
9	CTF-Th/ 50 mg	30 mL of Toluene/ACN (1:1), O_2, 3 h, AM 1.5 G simulated sunlight	Toluene	0.7	[3]
10	g-C_3N_4/ 20 mg	Ethanol/H_2O (9:1), O_2, 12 h, 300 W Xe-lamp, λ>420 nm	Ethanol	0.13	[4]
11	NCN/ 20 mg	Lactic acid, O_2, 5 h, 300 W Xe-lamp	Lactic acid	32.80	[5]
12	DCM-HCPs/ 10 mg	0.2 mmol benzylamine, 10 mL ACN, Air, 1.5 h, 455 nm Blue LED lamp	Benzylamine	5.71	[6]
13	H_3LP-HCPs/ 10 mg	0.2 mmol of benzylamine, 10 mL CH_3CN, air, 0.83 h, 455 nm Blue LED	Benzylamine	9.20	[7]
14	H_6P-HCPs/ 15 mg	BA/H_2O (2:3), O_2, 3h, 300 W Xe-lamp λ>420 nm	Benzyl alcohol	29.26	[8]
15	COF-JLU52/ 5 mg	Water: benzyl alcohol (9:1), AM1.5G simulated sunlight, O_2	Benzyl alcohol	7.62	[25]
16	TAPD-$(Me)_2$/ 20 mg	water: ethanol (9:1), 16 h, 250 W lamp	Ethanol	0.097	[26]
17	CTF-BDDBN/ 30 mg	Water: methanol (5 mL), 8 h, 300 W Xe lamp λ>420 nm	Methanol	0.15	[27]
18	DMCR-1NH/ 5 mg	10:1 water/IPA, 3 h, 300 W Xe lamp λ>420 nm	IPA	1.8	[28]
19	DE7-M/ 5 mg	Water: formic acid (9:1) 1.5 h, AM1.5G simulated sunlight	Formic acid	2.27	[29]

Table S3: Optimization conditions for the synthesis of Porp-Tz.

S.No	Solvent	Reaction Conditions	BET S.A. (m^2g^{-1})
1	Mesitylene: 1,4-Dioxane: 6 M AcOH (1:2:0.3)	120 °C, 3 days	29
2	o-DCB: n-Butanol: 6 M AcOH (1:1:0.3)	120 °C, 3 days	47
3	o-DCB: n-butanol: 6 M AcOH (1.5:1:0.2)	120 °C, 3 days	50
4	o-DCB: n-butanol: 6 M AcOH (3:1:0.3)	120 °C, 3 days	58
5	o-DCB: n-butanol: 6 M AcOH (2:1:0.3)	120 °C, 3 days	90
6	o-DCB: n-butanol: 8 M AcOH (2:1:0.3)	120 °C, 3 days	110
7	**o-DCB: n-butanol: 8 M AcOH (1:1:0.2)**	**120 °C, 4 days**	**186**

Reaction conditions: Porp-NH_2 (1 eq.); Tz-CHO (2 eq.); sealed under an inert atmosphere; and S.A.

Table S4: Wavelength-dependent AQY% for H_2O_2.

S. No	Wavelength λ (nm)	Intensity (Wcm^{-2})	Amount of H_2O_2 (µmol)	AQY (%)
1.	400	0.0014	12	6.21
2.	**420**	**0.0007**	**8**	**7.9**
3.	450	0.00184	6.88	2.4
4.	500	0.00266	12.5	2.7
5.	550	0.0037	9.7	1.37
6.	600	0.0137	9.5	0.34

Conditions: Porp-Tz (5 mg); Light source- 400 W Xenon lamp using bandpass filters of different wavelength; Irradiation time (t = 1 h); Irradiation area = 23 cm^2

References

1 B. Ge, Y. Ye, Y. Yan, H. Luo, Y. Chen, X. Meng, X. Song and Z. Liang, *Inorg. Chem.*, 2023, **62**, 19288–19297.

2 J. Luo, X. Wei, Y. Qiao, C. Wu, L. Li, L. Chen and J. Shi, *Adv. Mater.*, 2023, **35**, 2210110.

3 S. Kumar, B. Bayarkhuu, H. Ahn, H. Cho and J. Byun, *Nano Trends*, 2023, **4**, 100023.

4 Y. Shiraishi, S. Kanazawa, Y. Sugano, D. Tsukamoto, H. Sakamoto, S. Ichikawa and T. Hirai, *ACS Catal.*, 2014, **4**, 774–780.

5 H. Zhao, J. Yang, M. Eisapour, J. Hu and Z. Chen, *Chem. Eng. J.*, 2024, **490**, 151767.

6 W. Wang, W. Gao, X. Nie, W. Liu, X. Cheng, N. Shang, S. Gao and C. Wang, *J. Colloid Interface Sci.*, 2022, **616**, 1–11.

7 W. Gao, Y. Fu, X. Nie, Y. Zhao, C. Sun, N. Shang, X. Cheng, S. Gao, B. Tian and C. Wang, *ChemPhotoChem*, 2024, **n/a**, e202300294.

8 Y. Fu, Y. Xie, Y. Zhao, N. Shang, C. Sun, X. Cheng, W. Gao, S. Gao, B. Tian and C. Wang, *Eur. Polym. J.*, 2024, **210**, 112945.

9 A. Behera, A. K. Kar and R. Srivastava, *Inorg. Chem.*, 2022, **61**, 12781–12796.

10 X. Chen, Y. Kuwahara, K. Mori, C. Louis and H. Yamashita, *ACS Appl. Energy Mater.*, 2021, **4**, 4823–4830.

11 X. Chen, Y. Kuwahara, K. Mori, C. Louis and H. Yamashita, *J. Mater. Chem. A*, 2020, **8**, 1904–1910.

12 Y. Wu, X. Deng, R. Cui, M. Song, X. Guo, X. Gong, J. He and P. Chen, *J. Colloid Interface Sci.*, 2024, **656**, 528–537.

13 Z. Tian, C. Han, Y. Zhao, W. Dai, X. Lian, Y. Wang, Y. Zheng, Y. Shi, X. Pan, Z. Huang, H. Li and W. Chen, *Nat. Commun.*, 2021, **12**, 2039.

14 Z. Zheng, F. Han, B. Xing, X. Han and B. Li, *J. Colloid Interface Sci.*, 2022, **624**, 460–470.

15 Y. Shiraishi, S. Kanazawa, D. Tsukamoto, A. Shiro, Y. Sugano and T. Hirai, *ACS Catal.*, 2013, **3**, 2222–2227.

16 J. Zhang, L. Zheng, F. Wang, C. Chen, H. Wu, S. A. K. Leghari and M. Long, *Appl. Catal. B Environ.*, 2020, **269**, 118770.

17 L. Li, X. Huo, S. Chen, Q. Luo, W. Wang, Y. Wang and N. Wang, *Small*, 2023, **19**, 2301865.

18 C. Chen, G. Qiu, T. Wang, Z. Zheng, M. Huang and B. Li, *J. Colloid Interface Sci.*, 2021, **592**, 1–12.

19 D. Chen, W. Chen, Y. Wu, L. Wang, X. Wu, H. Xu and L. Chen, *Angew. Chemie Int. Ed.*, 2023, **62**, e202217479.

20 S. Chai, X. Chen, X. Zhang, Y. Fang, R. S. Sprick and X. Chen, *Environ. Sci. Nano*, 2022, **9**, 2464–2469.

21 M. Kou, Y. Wang, Y. Xu, L. Ye, Y. Huang, B. Jia, H. Li, J. Ren, Y. Deng, J. Chen, Y. Zhou, K. Lei, L. Wang, W. Liu, H. Huang and T. Ma, *Angew. Chemie Int. Ed.*, 2022, **61**, e202200413.

22 W. Zhao, P. Yan, B. Li, M. Bahri, L. Liu, X. Zhou, R. Clowes, N. D. Browning, Y. Wu, J. W. Ward and A. I. Cooper, *J. Am. Chem. Soc.*, 2022, **144**, 9902–9909.

23 Y. Shiraishi, T. Takii, T. Hagi, S. Mori, Y. Kofuji, Y. Kitagawa, S. Tanaka, S. Ichikawa and T. Hirai, *Nat. Mater.*, 2019, **18**, 985–993.

24 H. Xu, Y. Wang, Y. Xu, Q. Wang, M. Zhuang, Q. Liao and K. Xi, *Angew. Chemie Int. Ed.*, 2024, **n/a**, e202408802.

25 Z. Zhang, Q. Zhang, Y. Hou, J. Li, S. Zhu, H. Xia, H. Yue and X. Liu, *Angew. Chemie Int. Ed.*, 2024, **n/a**, e202411546.

26 C. Krishnaraj, H. Sekhar Jena, L. Bourda, A. Laemont, P. Pachfule, J. Roeser, C. V. Chandran, S. Borgmans, S. M. J. Rogge, K. Leus, C. V Stevens, J. A. Martens, V. Van Speybroeck, E. Breynaert, A. Thomas and P. Van Der Voort, *J. Am. Chem. Soc.*, 2020, **142**, 20107–20116.

27 L. Chen, L. Wang, Y. Wan, Y. Zhang, Z. Qi, X. Wu and H. Xu, *Adv. Mater.*, 2020, **32**, 1904433.

28 P. Das, G. Chakraborty, J. Roeser, S. Vogl, J. Rabeah and A. Thomas, *J. Am. Chem. Soc.*, 2023, **145**, 2975–2984.

29 L. Liu, M.-Y. Gao, H. Yang, X. Wang, X. Li and A. I. Cooper, *J. Am. Chem. Soc.*, 2021, **143**, 19287–19293.